IJNAOE
©SNAK, 2015

Int. J. Nav. Archit. Ocean Eng. (2015) 7:979~994
http://dx.doi.org/10.1515/ijnaoe-2015-0068
pISSN: 2092-6782, eISSN: 2092-6790

Extraction of the mode shapes of a segmented ship model with a hydroelastic response

Yooil Kim[1], In-Gyu Ahn[1] and Sung-Gun Park[2]

[1]*Department of Naval Architecture and Ocean Engineering, Inha University, Incheon, Korea*
[2]*DSME R&D Institute, Daewoo Shipbuilding and Marine Engineering Co.,Ltd., Seoul, Korea*

Received 29 May 2015; Revised 31 July 2015; Accepted 3 August 2015

ABSTRACT: *The mode shapes of a segmented hull model towed in a model basin were predicted using both the Proper Orthogonal Decomposition (POD) and cross random decrement technique. The proper orthogonal decomposition, which is also known as Karhunen-Loeve decomposition, is an emerging technology as a useful signal processing technique in structural dynamics. The technique is based on the fact that the eigenvectors of a spatial coherence matrix become the mode shapes of the system under free and randomly excited forced vibration conditions. Taking advantage of the simplicity of POD, efforts have been made to reveal the mode shapes of vibrating flexible hull under random wave excitation. First, the segmented hull model of a 400 K ore carrier with 3 flexible connections was towed in a model basin under different sea states and the time histories of the vertical bending moment at three different locations were measured. The measured response time histories were processed using the proper orthogonal decomposition, eventually to obtain both the first and second vertical vibration modes of the flexible hull. A comparison of the obtained mode shapes with those obtained using the cross random decrement technique showed excellent correspondence between the two results.*

KEY WORDS: Hydroelasticity; Mode shape; Proper orthogonal decomposition; Cross random decrement.

INTRODUCTION

The structural safety of large seagoing merchant ships is threatened by the presence of a hydroelastic hull girder response, i.e. springing and whipping. To improve the understanding on this complicated fluid-structure interaction problem, eventually minimizing the risks that may be taken by ship designers and owners, considerable research efforts have been devoted over the past decade. Most research activities in this area may be classified into two categories, i.e., computational method and experimental methods. The recent achievements of the computation method on the hydroelasticity (Price and Temarel, 1982; Jensen and Dogliani, 1996; Wu and Moan, 1996; Malenica et al., 2003; Hirdaris et al., 2003; Iijima et al., 2008; Kim et al., 2009; Kim et al., 2013; Malenica et al., 2013; Senjanovic et al., 2014) have been rather dramatic due to the rapid increase in computational power. On the other hand, both model basin test and full scale measurement have also been actively conducted due to the limitations of the computation method (Remy et al., 2006; Iijima et al., 2009; Miyake et al., 2009; Oka et al., 2009; Hong et al., 2011). Whatever the methodology is, the dynamic modal parameters, such as natural frequencies, damping coefficients and

Corresponding author: *Yooil Kim*, e-mail: *yooilkim@inha.ac.kr*

This is an Open-Access article distributed under the terms of the Creative Commons Attribution Non-Commercial License (http://creativecommons.org/licenses/by-nc/3.0) which permits unrestricted non-commercial use, distribution, and reproduction in any medium, provided the original work is properly cited.

mode shapes, are of prime interest from the viewpoint of the dynamic response of a vibrating hull structure. Regarding the experimental method, without considering its scale, these dynamic modal parameters need to be extracted from the response of a vibrating ship structure because they are a priori unknowns. This becomes even more important when analyzing the full scale measurement data (Hirdaris et al., 2009; Miyake et al., 2010; Drummen et al., 2009; Jensen et al., 2009), where the dynamic modal parameters should be extracted from the measured response only. The output only approach is inevitable for the full scale measurement data due to the accuracy issue of the external excitation, i.e. incoming waves, which are not straightforward to measure for seagoing vessels.

Kim and Park (2013) examined the modal parameter identification of hydroelastically responding ship structure. They applied the so called random decrement technique to the measured Vertical Bending Moment (VBM) time history of a segmented hull model and extracted both the natural frequencies and damping ratios under wet towing conditions. They reported that the derived natural frequencies did not show any significant discrepancy compared to those obtained by still water wet hammering test results, but the damping ratios under wet towing conditions were up to 20% higher than those obtained by wet hammering test. Mariani and Dessi (2012) evaluated an estimation of the mode shapes of a vibrating hull structure on a small scale model. They applied the Proper Orthogonal Decomposition (POD) method to extract the mode shapes of a segmented hull model connected to a backbone structure running from bow to stern. The first, second and third vertical mode shapes were estimated by processing both the measured VBM and acceleration using POD, and they determined that both matched each other well. This paper is an extension of the work by Kim and Park (2013) targeting the identification of wet mode shapes of a segmented hull model using both the proper orthogonal decomposition method and Cross Random Decrement Technique (CRDT).

The POD is a statistics-based order reduction technique through which the motion of a dynamic system of large DOF can be approximated by the combination of lower order descriptions. The basic principle behind this method is that the eigenvector of a spatial coherence matrix of certain physical quantities measured at several different locations becomes the mode shapes, or basis function of the system, which may then be used in the Galerkin procedure. This is an important technique for data reduction, feature extraction, and it has been used widely in many engineering fields, such as image processing, signal analysis, system identification and adaptive control etc. The starting engineering application of the POD was based on an analysis of the spatial distribution of turbulence in a fluid field (Lumley, 1970), and later an extension was made toward the mode shape extraction of a vibrating structure (Feeny and Kappagantu, 1998; Feeny, 2002). Another interesting technique that can be used to extract the mode shapes is CRDT. This technique was developed originally by Cole (1968; 1971) in the form of an 'auto' random decrement to identify the dynamic characteristics and in-service damage detection of the space structure from the measured response only. Ibrahim and Mikulcik (1977) later introduced the concept of the cross random decrement signature that enabled the identification of the mode shapes of a multi-DOF system.

In this paper, efforts have been made to estimate the mode shapes of a segmented hull model towed in the model basin using both POD and CRDT. Regarding POD, the VBM time histories measured at different ship cross sections were processed and the spatial coherence matrix was obtained. The eigenvector of the coherence matrix was derived numerically, eventually becoming the mode shapes of the system under random excitation conditions. For CRDT, the cross random decrement signatures, which represent the free decay signal of the measured VBM at different locations, were derived by taking the conditional ensemble average of the signal under a certain triggering conditions. Successive ensemble averaging finally led to the converged free decay signal due to the randomness of the response with zero-mean Gaussianity.

THEORETICAL BACKGROUND

Proper orthogonal decomposition

The POD begins from the spatial coherence matrix of a certain physical quantity, the VBM at different locations in this particular case. The ensemble matrix of measured VBM at M different locations along the ship is defined in Eq. (1).

$$\mathbf{X} = [\mathbf{x}_1, \mathbf{x}_2, \mathbf{x}_3 ..., \mathbf{x}_M] \tag{1}$$

where the column vector, $\mathbf{x}_i$, stands for the VBM time history of N discrete time intervals, and can be represented by Eq. (2).

$$\mathbf{x}_i = [x_i(t_1), x_i(t_2), x_i(t_3)..., x_i(t_N)]^T \tag{2}$$

The equation of motion of a freely vibrating undamped multi DOF spring mass system is given as Eq. (3), where both $\mathbf{M}$ and $\mathbf{K}$ are the symmetric positive definite square matrix.

$$\mathbf{M}\ddot{\mathbf{x}} + \mathbf{K}\mathbf{x} = \mathbf{0} \tag{3}$$

The system's modal vectors are orthonormal with respect to the mass and stiffness matrix once normalized in such a way that $\mathbf{V^T M V = I}$ or $\mathbf{v}_i^T \mathbf{M} \mathbf{v}_j = \delta_{ij}$, where $\mathbf{V}$ is the normal mode matrix of the system. A coordinate transformation of $\mathbf{x} = \mathbf{M}^{-1/2}\mathbf{q}$ leads Eq. (3) to (4).

$$\ddot{\mathbf{q}} + \mathbf{M}^{-1/2}\mathbf{K}\mathbf{M}^{-1/2}\mathbf{q} = \mathbf{0} \tag{4}$$

The advantage of Eq. (4) lies on the fact that the stiffness matrices are still symmetrical and the mass matrix is the identity. Eq. (4) shows that the equation of motion can be transformed to an equivalent system, whose mass matrix is the identity one and its modal vector satisfies the orthonormality condition, i.e., $\mathbf{v}_i^T \mathbf{v}_j = \delta_{ij}$. Now suppose that the solution of Eq. (5) is given as a linear combination of the normal modes so that one has

$$\mathbf{x}(t) = e_1(t)\mathbf{v}_1 + e_2(t)\mathbf{v}_2 + \cdots + e_M(t)\mathbf{v}_M \tag{5}$$

where $e_i(t)$ is the time modulation of the i[th] mode. The ensemble matrix given in Eq. (1) has the form,

$$\mathbf{X} = [\mathbf{x}(t_1), \mathbf{x}(t_2), \cdots, \mathbf{x}(t_N)]^T = [\mathbf{e}_1\mathbf{v}_1^T + \mathbf{e}_2\mathbf{v}_2^T + \cdots + \mathbf{e}_M\mathbf{v}_M^T], \tag{6}$$

where the row vector $\mathbf{e}_i$ is defined as $[e_i(t_1), e_i(t_2), \cdots, e_i(t_N)]$. The spatial coherence matrix post multiplied by $\mathbf{v_j}$ gives,

$$\mathbf{R}\mathbf{v_j} = \frac{1}{N}\mathbf{X^T}\mathbf{X}\mathbf{v_j} = \frac{1}{N}[\mathbf{e}_1\mathbf{v}_1^T + \mathbf{e}_2\mathbf{v}_2^T + \cdots + \mathbf{e}_M\mathbf{v}_M^T]^T[\mathbf{e}_1\mathbf{v}_1^T + \mathbf{e}_2\mathbf{v}_2^T + \cdots + \mathbf{e}_M\mathbf{v}_M^T]\mathbf{v_j} \tag{7}$$

where the matrix, $\mathbf{R}$, is defined as a spatial coherence matrix, i.e. $\frac{1}{N}\mathbf{X^T}\mathbf{X}$. Each entry of the coherence matrix, R_{ij}, is the inner product of the two measured VBM time histories at locations i and j, which indicates the correlation of the VBM of two locations. Considering the orthonormality of the eigenvectors, the far right term of Eq. (7) becomes,

$$\mathbf{R}\mathbf{v_j} = \frac{1}{N}(\mathbf{v}_1\mathbf{e}_1^T\mathbf{e}_j + \mathbf{v}_2\mathbf{e}_2^T\mathbf{e}_j + \cdots \mathbf{v}_M\mathbf{e}_M^T\mathbf{e}_j) \tag{8}$$

All terms of Eq. (8) except for $\mathbf{v}_j\mathbf{e}_j^T\mathbf{e}_j$ will disappear because of the distinct frequency of each vibration mode when the signal record length is long enough. Hence,

$$\lim_{N\to\infty}\frac{1}{N}\mathbf{v}_i\mathbf{e}_i^T\mathbf{e}_j = 0 \quad \textit{when } i \neq j \tag{9}$$

Taking advantage of Eq. (9), Eq. (8) finally becomes,

$$\mathbf{Rv_j} = \frac{\mathbf{e}_i^T \mathbf{e}_j}{N} \mathbf{v}_j = \lambda \mathbf{v}_j \tag{10}$$

Eq. (10) implies that the eigenvectors of the coherence matrix, $\mathbf{R}$, which is called the Proper Orthogonal Mode (POM), becomes the modal vector of the given system that the measurement was made on. The relationship given as Eq. (10) holds only if the mass matrix is known, otherwise the orthonomality condition of the eigenvectors cannot be utilized. On the other hand, it also has been highlighted by several authors that the most excited mode can always be obtained based on Eq. (10), even in the case that the mass matrix is unknown, which is usually the case (Mariani and Dessi, 2012).

Eq. (10) holds only when the external excitation is absent, i.e., free vibration case, but most of the real world situations is a forced vibration. In the case that the external harmonic excitation is present, different mode shapes may be excited with the same frequency so that Eq. (9) would not hold any longer. Nevertheless, if one of the modes resonates with a predominantly large magnitude, the POM becomes a good approximation of the mode shape. The accuracy of the approximation depends strongly on the relative magnitude of the resonant vibration and non-resonant one. The hydroelastic response of a flexible ship is a resonance dominant one with relatively small damping, which can be confirmed in the frequency domain with sharp peaks right on the natural frequency of the system. Therefore, the derived POMs based on Eq. (10) is a good approximation of the mode shapes of vibrating ship structure.

Random decrement technique

The random decrement technique is a simple but very powerful method for identifying a dynamic system, and is used widely for modal parameter identification, where prior information on excitation is unknown. Assuming that the signals, $x(t)$ and $y(t)$, represent VBM at two different locations along the ship length, the auto and cross random decrement signature is defined as the expected value of the given signal $x(t)$ under certain conditions, which are denoted as $T_{x(t)}$.

$$D_{xx}(\tau) = E[x(t+\tau) \mid T_{x(t)}]$$

$$D_{xy}(\tau) = E[y(t+\tau) \mid T_{x(t)}] \tag{11}$$

$D_{xx}(\tau)$ is the auto random decrement signature and $D_{xy}(\tau)$ is the cross random decrement signature, and they both become the free decay signal at two different locations, x and y. The idea behind Eq. (11) is to cancel out the particular solution of the dynamic response of a given system by taking the conditional average across a large number of ensembles, leaving the homogeneous solution to be averaged. While taking the average across the ensembles, a certain condition is imposed so that the cancellation can be achieved with a finite number of ensembles.

Assuming that the process is ergodic, which means the stationarity of the process, Eq. (11) can be rewritten as Eq. (12). Hence, the conditional averaging across the ensembles can be made within a single sample realization.

$$D_{xx}(\tau) = \frac{1}{N}\sum_{i=1}^{N} x(t_i+\tau) \mid T_{x(t_i)}$$

$$D_{xy}(\tau) = \frac{1}{N}\sum_{i=1}^{N} y(t_i+\tau) \mid T_{x(t_i)} \tag{12}$$

where N is the number of points in the random process that satisfy the condition, $T_{x(t)}$. The condition, $T_{x(t)}$, under which the mean values of $x(t)$ and $y(t)$ are taken, is called the triggering condition, and there are several different types, such as level

crossing triggering, local extremum triggering, positive point triggering, and zero crossing triggering, etc. In this study, the level crossing triggering condition was applied to extract the free decay signal from the measured one owing to its simplicity, and can be rewritten in a general form as Eq. (13).

$$T_{x(t)}^{T} = \{a \le x(t) < a + \Delta a, -\infty \le \dot{x}(t) < \infty\} \tag{13}$$

where a is the triggering level and Δa is the triggering range, which was set to be infinitesimally small. If the triggering range, Δa, becomes finite, the level crossing triggering becomes positive point triggering.

EXPERIMENT

In the experimental study, the scaled segmented model of the Very Large Ore Carrier (VLOC) of a 400,000 ton dead weight was tested in the model basin. Table 1 lists the main particulars of the tested ship.

Table 1 Main characteristics of the 400,000 DWT ore carrier.

Items	Full scale	Model scale
Length between perpendiculars [*m*]	350.00	5.83
Breadth molded [*m*]	65.00	1.08
Depth molded [*m*]	30.40	0.51
Displacement [*tones*] – Normal ballast	209,623	0.97
Mean draft [*m*]	11.44	0.19

Fig. 1 shows the test model floating on the undisturbed free surface (Selvik, 2010). The scale of the model, i.e., the ratio of the length dimension between the model and full scale ship was 1/60, which was determined based on the minimum wave quality of the model basin. The Froude scale law was applied to scale-down both the length and time. Therefore, the Froude numbers of the full and model scales were set to be same as Eq. (14).

$$\frac{V_m}{\sqrt{gL_m}} = \frac{V_f}{\sqrt{gL_f}} \tag{14}$$

where V_m and V_f are the speed of the model and full scale ship, respectively. L_m and L_f are the length of the model and full scale ship, respectively, and g is the gravitational acceleration. The relationship between the full and model scales gives the speed of the model as well as the frequency of the waves, as expressed in Eq. (15).

$$V_m = V_f \sqrt{\frac{L_m}{L_f}} = V_f \sqrt{\Lambda}$$

$$\omega_m = \omega_f \sqrt{\frac{L_f}{L_m}} = \omega_f \sqrt{\frac{1}{\Lambda}} \tag{15}$$

where ω_m and ω_f are the wave frequency of the model and full scale, respectively, and Λ is the scale ratio. The scaling of

the flexibility is obtained by combining the frequency of a homogeneous beam and the wave frequency relation given in Eq. (15). Therefore, the bending stiffness of the model is

$$EI_m = EI_f \frac{\rho_m}{\rho_f \Lambda^5} \tag{16}$$

where EI is the bending stiffness and ρ is the density of the material.

The entire hull is divided into 4 rigid sections. Three adjustable flexible connections, at L/4, 2L/4 and 3L/4, were placed between the sections so that the flexibility of the ship could be reproduced accurately in the scaled model. Only the vertical bending flexibility was considered in the model because the vibratory response of a hull is expected to be the maximum when it moves forward across the head wave. The mass distribution of the real ship was also reflected in the model by adjusting the location of a mass block inside the model. Load cells were installed with connections and the VBM and shear forces were measured during the test with its sampling frequency to be 400 *Hz*.

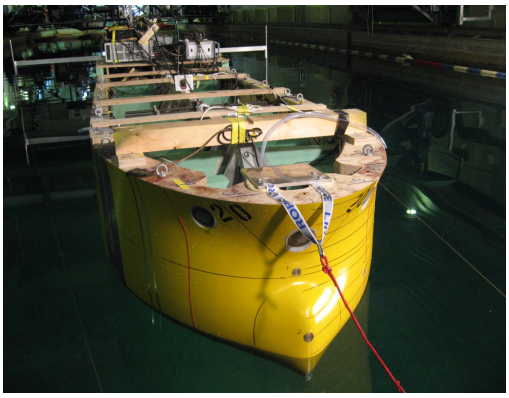

(a) Test model in a model basin.

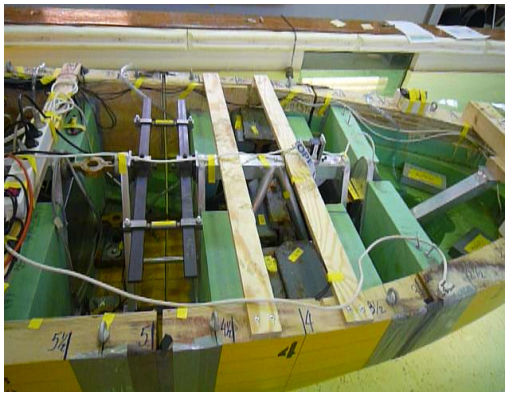

(b) Connecting part between the segments.

Fig. 1 Test model (1/60 scale).

In order for the scaled model to be the representative of the real ship structure, the dynamic characteristics of the full scale ship, such as the natural frequencies and damping ratio, need to be realized accurately in the model test. The expected wet natural frequencies of the model under ballast conditions was 0.48 *Hz* and 0.98 *Hz* for the first and second vertical vibration modes, respectively, according to the Froude scale law. The stiffness of the adjustable flexible connections was changed until the wet natural frequency of the model matched the target value. The wet natural frequencies of the model were obtained using a wet hammering test, i.e., hitting the stern of the model with an impact load. The actual wet natural frequencies of the first and second vertical modes achieved through the wet hammering test were 0.47 *Hz* and 1.07 *Hz*, respectively. Because the first vertical mode is the most influential, the match between the target and achieved wet natural frequency of the first vertical mode was considered most important. No intentional calibration was made for the damping ratio of the model because the damping ratio of the full scale ship is unknown. The damping ratio that was derived from the hammering test was approximately 0.4~0.6% under wet conditions. A part of it was structural damping and the remaining part is hydrodynamic damping. The model ship was towed in the model basin, where the waves of given spectra are generated. The wave spectra are in the form of the JONSWAP spectrum (DNV, 2000), with its parameters are set to be $\gamma = 1$, $H_s = 2.5\ m$, $T_p = 9.2$ sec, $V = 14.5\ kts$. The test was carried out for a minimum of 40 minutes in the model scale time, which is long enough to derive meaningful statistical values.

Fig. 2 shows a part of the bending moment time history at L/4 for a sea state. Fig. 2(a) shows the measured time history, where the mean static bending moment was removed, and Fig. 2(b) and (c) present the filtered signal with the frequency bands covering both the first and second natural frequencies of the model ship.

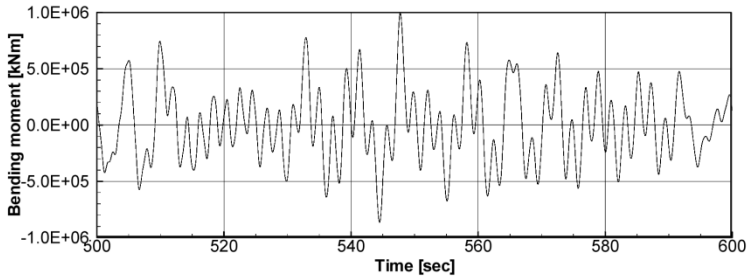

(a) VBM time history.

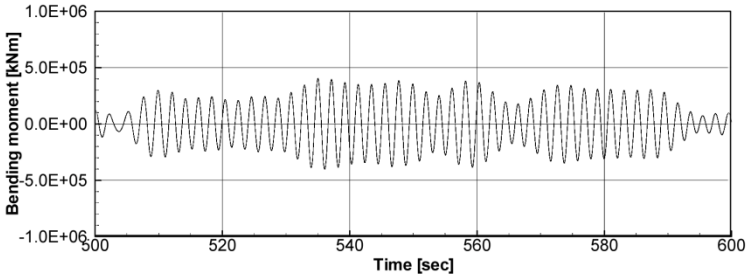

(b) Filtered VBM time history (0.35 *Hz*<f<0.8 *Hz*).

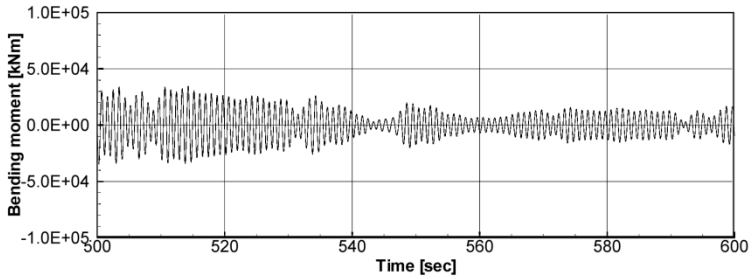

(c) Filtered VBM time history (0.8 *Hz*<f<3.0 *Hz*).

Fig. 2 Bending moment time history at L/4.

MODE SHAPE EXTRACTION

Proper orthogonal decomposition

The eigenvectors of the vibrating hull structure were derived using the relationship between the spatial coherence matrix and the system's eigenvectors given as Eq. (10). A total of 3 eigenvectors could be derived from eigenvalue analysis because the spatial variation of the vertical bending moment was measured at three discrete points.

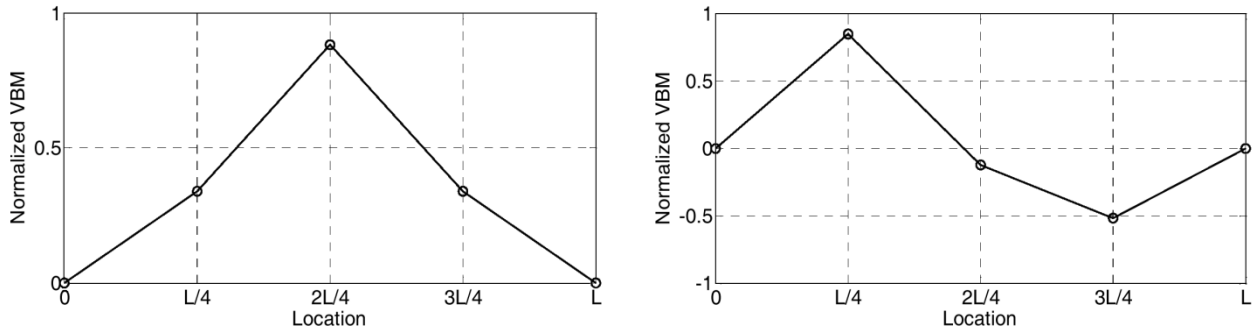

(a) 1st mode. (b) 2nd mode.

Fig. 1 Mode shapes calculated by POD method.

On the other hand, due to the limited number of segmentations of the hull, the 4 node vertical bending vibration mode was almost absent so that only 2 and 3 node vibrations were considered. Fig. 3 shows the mode shapes of the vertical bending moment obtained using the POD. The 1st and 2nd modes corresponds to 2 node and 3 node vertical bending modes, respectively.

Fig. 4 shows the time history of the decomposed vertical bending moments for both 1st and 2nd modes, which were reconstructed using the obtained eigenvectors and eigenvalues. Decomposition of the signal is based on the relationship given in Eq. (5), where the total system response is expressed as the summation of each mode shape multiplied by the corresponding principal coordinate. The time evolution of each mode can be derived easily by projecting the total system response to each modal vector, which is orthogonal to all the others. At the midship location, the magnitude of the vertical bending moment of the 1st mode is the largest among others, whereas it becomes almost zero for the 2nd mode, as expected, considering the deformation shape of 3 node vibration mode of the free-free beam-like structure. An interesting aspect of the 2nd mode is that the vertical bending moment at L/4 is slightly larger than that at 3L/4 meaning that the perfect symmetry is violated in terms of the curvature, which can also be seen in the identified mode shape given in Fig. 3(b).

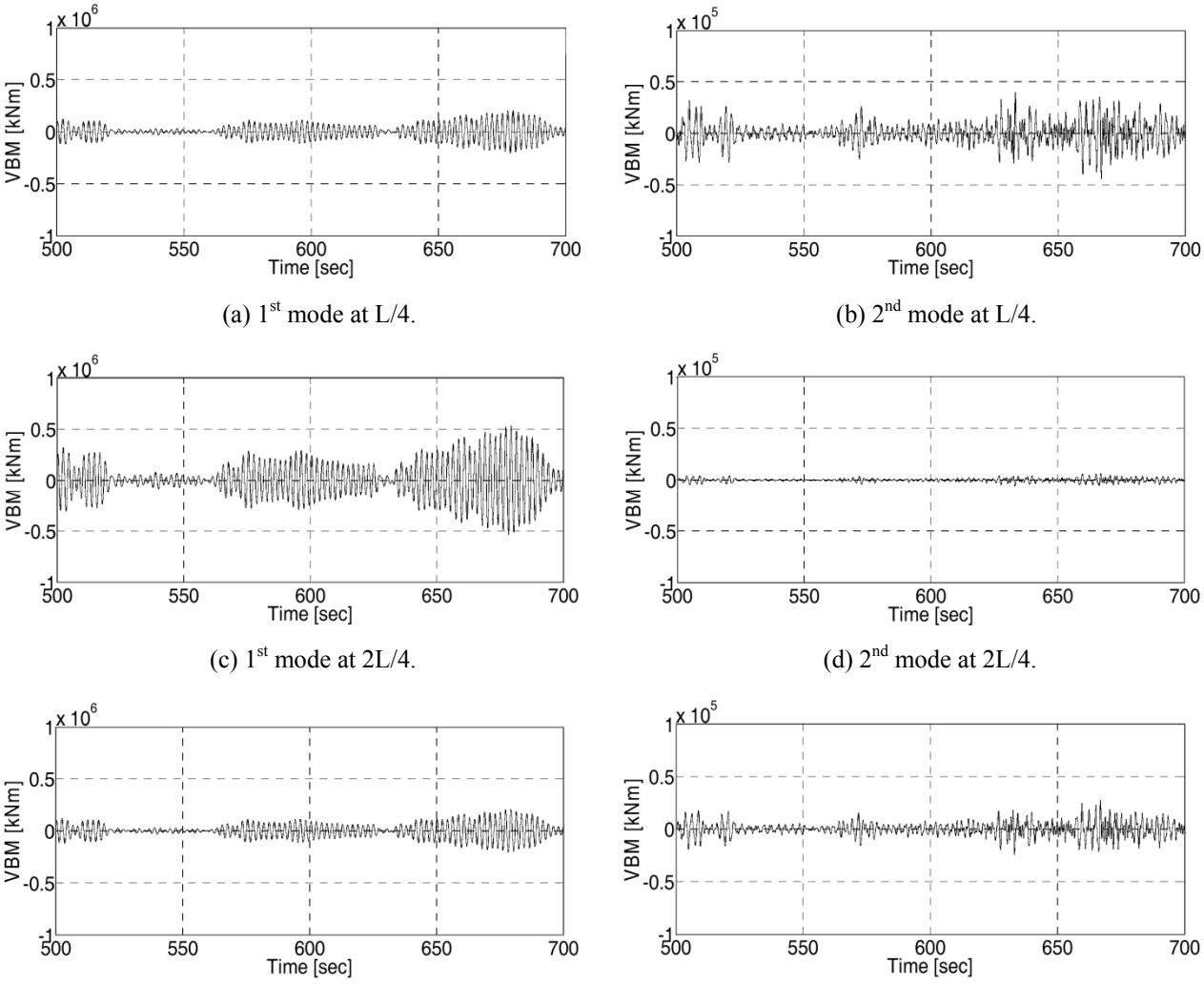

(a) 1st mode at L/4. (b) 2nd mode at L/4.

(c) 1st mode at 2L/4. (d) 2nd mode at 2L/4.

(e) 1st mode at 3L/4. (f) 2nd mode at 3L/4.

Fig. 4 Decomposed VBM time history at L/4, 2L/4 and 3L/4.

Fig. 5 compares the time history of the measured vertical bending moment at three different locations with that of reconstructed one by adding the 1st and 2nd mode shapes decomposed by the POD method. The two results compares quite well with slight deviations, which means that modes higher than the 2nd one are negligible.

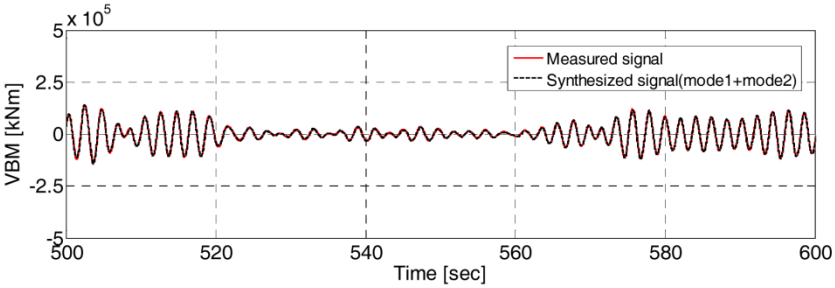

(a) at L/4.

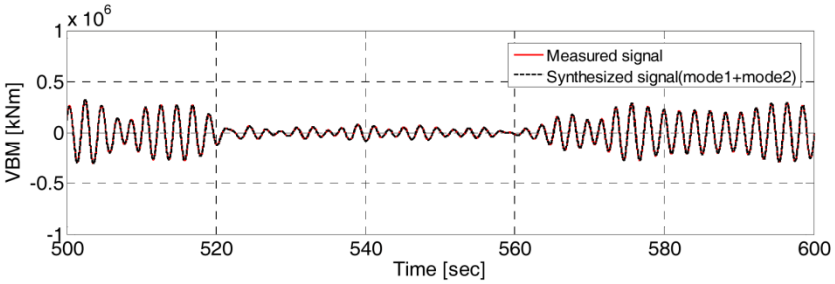

(b) at 2L/4.

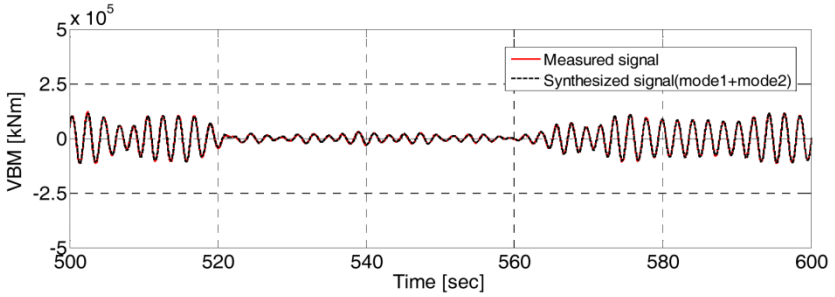

(b) at 3L/4.

Fig. 5 Comparison between the measured VBM time history and synthesized one at L/4, 2L/4 and 3L/4.

The accuracy of POM can be validated by checking the relative contributions of the terms of Eq. (8), or the condition given as Eq. (9). Table 2 lists the absolute values of the three terms of $\frac{1}{N}e_i^T e_j$ for each mode, i.e., $i = 1, 2$. As indicated by Eq. (9), the terms with $i \neq j$ should be as minimal as possible, so the term with $i = j$ should prevail over the others. Table 2 confirms that the two terms with $i \neq j$ are negligibly small compared to the terms with $i = j$, and the value matches well with the eigenvalues of the coherence matrix. Table 2 also shows numerically the validity of POD even in cases when the mass distribution is unknown and the vibration is a forced one.

Table 2 Error analysis of POD.

	i	j	λ	$\frac{1}{N}e_i^T e_j$
1st mode	1	1	9.6320×10^{10}	9.4715×10^{10}
	1	2		1.3299×10^{-5}
	1	3		-1.5447×10^{-5}
2nd mode	2	1	3.9404×10^{8}	1.3299×10^{-5}
	2	2		3.8747×10^{10}
	2	3		1.0285×10^{-5}

Cross random decrement technique

As defined in Eq. (11), the cross random decrement technique was used to extract the mode shapes of a vibrating hull. First of all, the measured vertical bending moment time history was filtered using a band pass filter, so that the signal of each vibration mode was decomposed and processed further. Fig. 6(a) shows the measured vertical bending moment time history at the L/4 location, and Fig. 6(b) shows the band pass filtered signal with a frequency band of 0.35 *Hz*<f<0.8 *Hz*, which corresponds to the first vibration mode. The marks in Fig. 6(b) indicate the triggering points of level crossing triggering, which are set to be the standard deviation of the entire signal. Based on these triggering points, a certain length of signal was selected and averaged, assuming that the process is stationary and ergodic. Fig. 6(c) shows the band pass filtered signal with its frequency band of 0.8 *Hz*<f<3 *Hz*, which corresponds to the second mode. The upper limit of the band pass filter for the second mode may be chosen arbitrarily because there are no further higher vibration modes other than the second mode in this particular case.

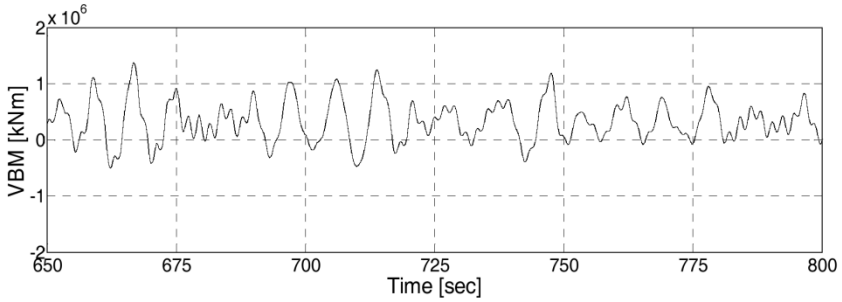

(a) VBM time history at L/4.

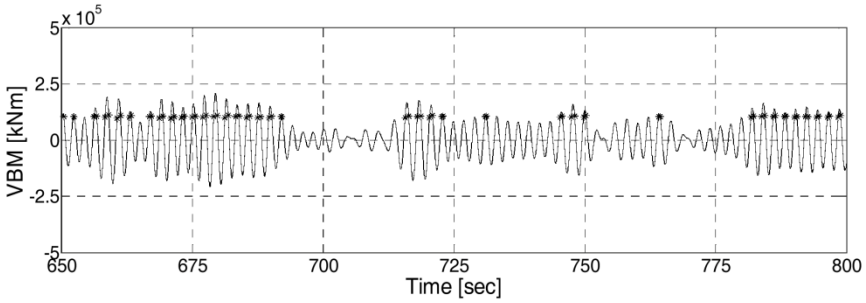

(b) Filtered VBM time history (0.35 *Hz*<f<0.8 *Hz*) and triggering points.

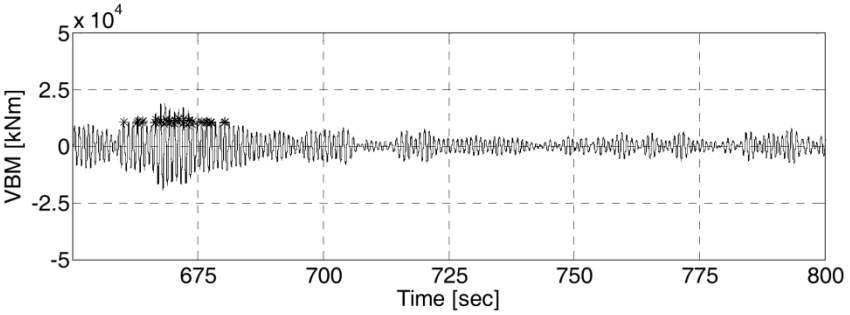

(c) Filtered VBM time history (0.8 *Hz*<f<3.0 *Hz*) and triggering points.

Fig. 6 Filtered and unfiltered VBM time history at L/4 with triggering points.

Fig. 7 presents the evolution of CRDS with respect to the number of ensembles at three different locations along the ship length. As shown in Fig. 7, the CRDS converges and stabilizes quickly so that no further change can be observed under further averaging. To check the convergence of the shape of the free decay signal, each ensemble chosen out of the original signal was normalized to the length of signal itself before taking the average. In case of a normalized signal of 2L/4 for the

second mode, as shown in Fig. 7(d), the peaks of the signal were fluctuating rather than smoothly decaying, which is the case for all others. This is because the absolute bending moment values remains near zero at 2L/4 for the second mode throughout the entire time span because of the deformation shape of this particular mode, which leads to relatively large errors for the decaying pattern. Fig. 8 shows the evolution of error with respect to the number of ensemble averages, where the error is defined by Eq. (17).

$$Error(n) = \frac{\left\| D_{xy}^{n}(\tau) - D_{xy}^{n-1}(\tau) \right\|}{\left\| D_{xy}^{n-1}(\tau) \right\|} \times 100[\%] \tag{17}$$

where n means the number of samples used for averaging and $\|\cdot\|$ means vector norm. For all three locations, where the bending moment was measured, the error decayed quickly and became less than 5% when the number of samples reached 100. Again, the convergence pattern of the error at 2L/4 of the second mode was different from other cases due to the small absolute value of the bending moment.

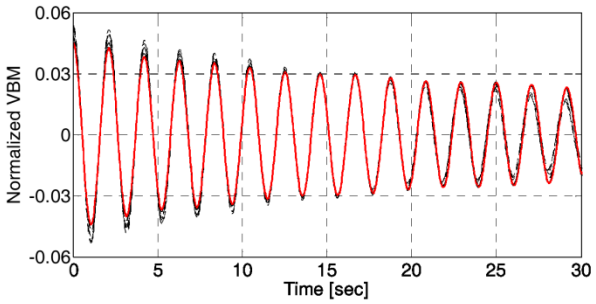

(a) at L/4 – 1st mode.

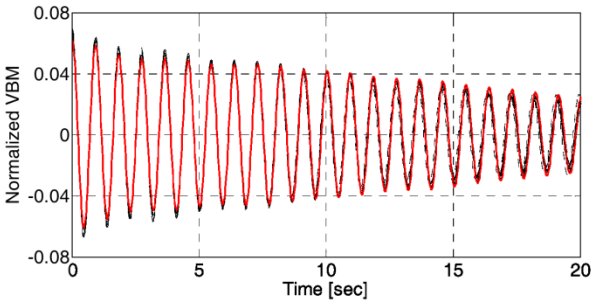

(b) at L/4 – 2nd mode.

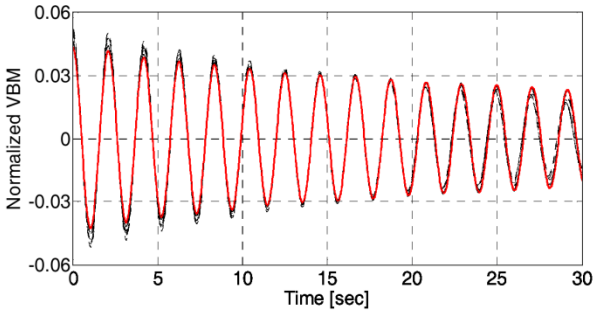

(c) at 2L/4 – 1st mode.

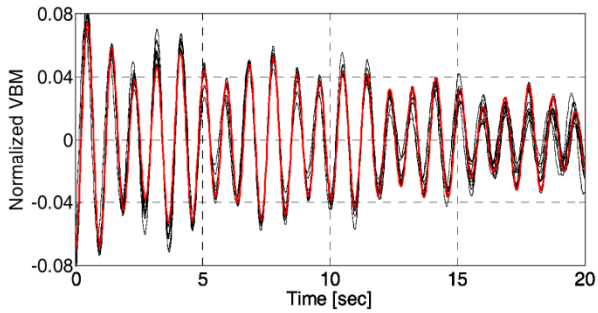

(d) at 2L/4 – 2nd mode.

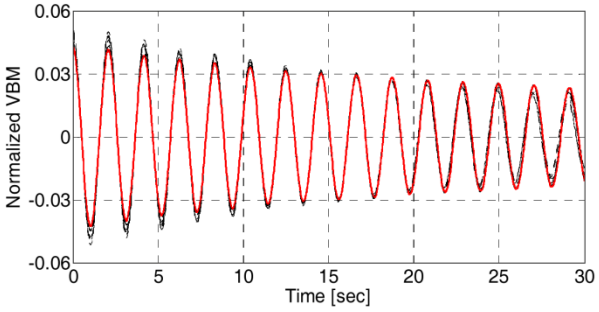

(e) at 3L/4 – 1st mode.

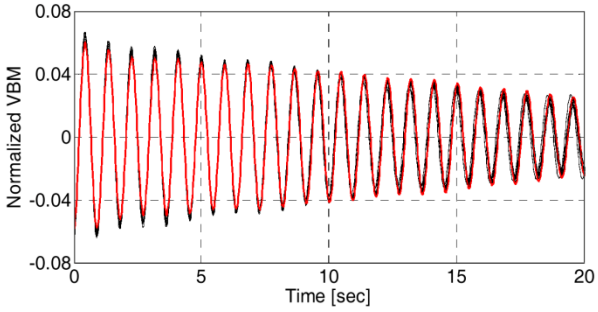

(f) at 3L/4 – 2nd mode.

Fig. 7 Convergence of VBM CRDS at L/4, 2L/4 and 3L/4 (1st mode).

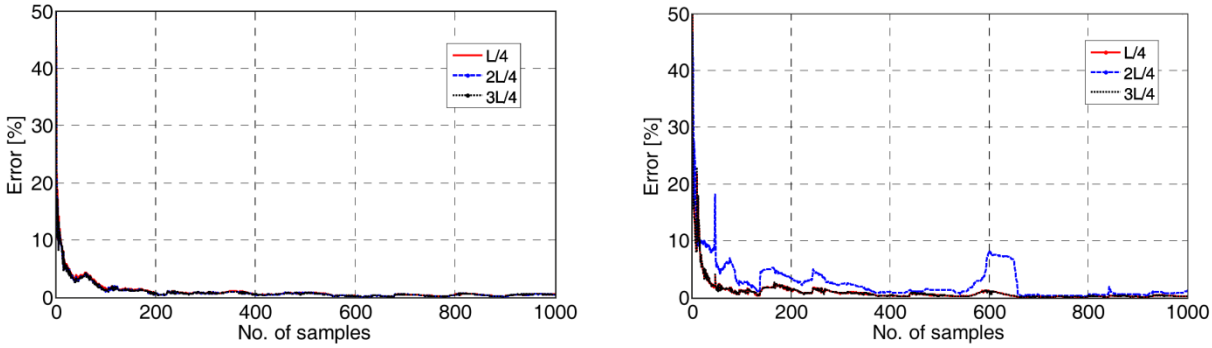

(a) 1st mode. (b) 2nd mode.

Fig. 8 Error convergence of CRDS at L/4, 2L/4 and 3L/4.

Fig. 9 shows the converged CRDS at three different locations, for both the first and second modes. For the first mode, the vertical bending moment oscillated in the same frequency without any phase lag between them as expected. In addition, the magnitudes of the vertical bending moment at L/4 and 3L/4 matched precisely, whereas that at 2L/4 was higher than the other two. In the case of the second mode, the vertical bending moments at L/4 and 3L/4 were out of phase with their magnitudes comparable to each other. The magnitude at 2L/4 remained near zero, implicitly demonstrating the deformation shape of the second mode.

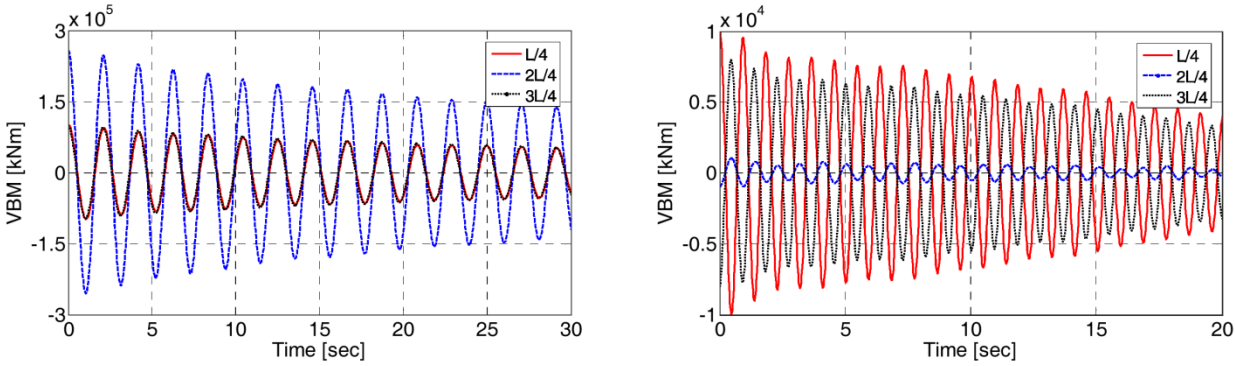

(a) 1st mode. (b) 2nd mode.

Fig. 9 Converged CRDS at L/4, 2L/4 and 3L/4.

Fig. 10 presents the longitudinal distribution of the vertical bending moment for the arbitrarily chosen time instances. The solid red line is the envelope of the bending moment distribution along the ship length. The envelope was segmented because the bending moments were measured at three discrete location, as shown in Fig. 10. The bending moments at the two end locations were assumed to be all zeros.

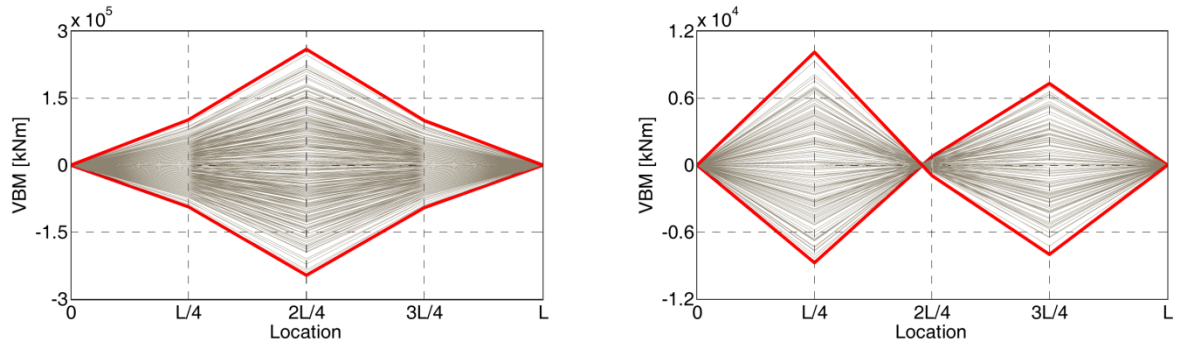

(a) 1st mode. (b) 2nd mode.

Fig. 10 Time evolution of the vertical bending moment along the ship length.

Fig. 11 shows the longitudinal distribution of the curvature, slope and deflection for both the first and second mode. The longitudinal distribution of curvature was identical to that of the bending moment due to the linear relationship between the two. The slope can be obtained by integrating the curvature following the geometrical relationship, and the deflection by integrating the slope. Simple trapezoidal rule was employed for this spatial integration. While integrating the curvature to obtain the slope, the points were connected to the line segment. The obtained deflection was corrected by rotating the ship so that the deflection at both ends of the ship becomes zero. For both the first and second modes, the shapes of the deflection were the normally observed ones.

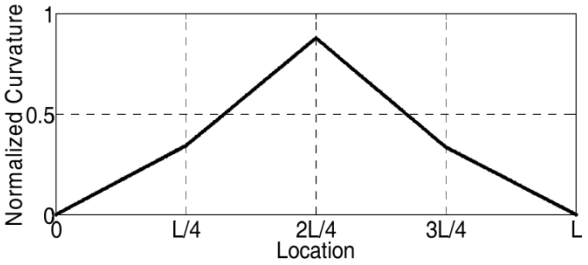

(a) Curvature – 1st mode.

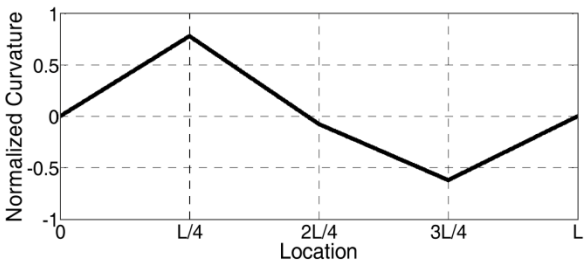

(b) Curvature – 2nd mode.

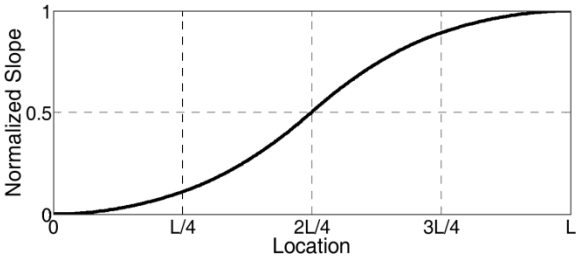

(c) Slope – 1st mode.

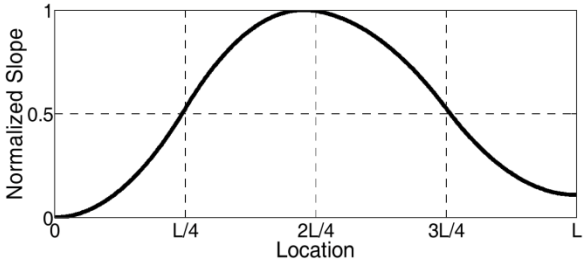

(d) Slope – 2nd mode.

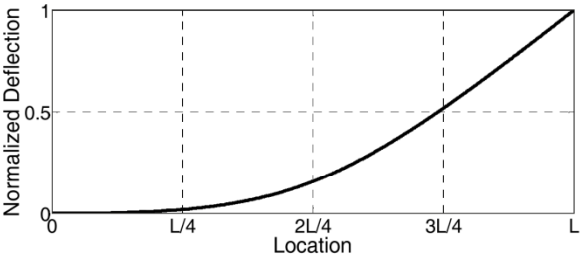

(e) Deflection – 1st mode.

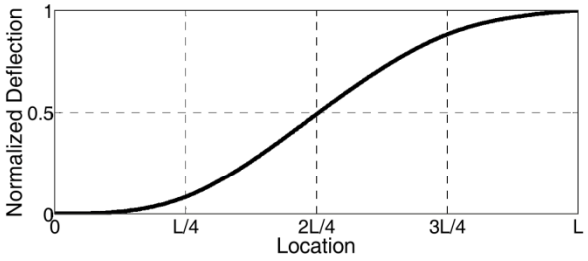

(f) Deflection – 2nd mode.

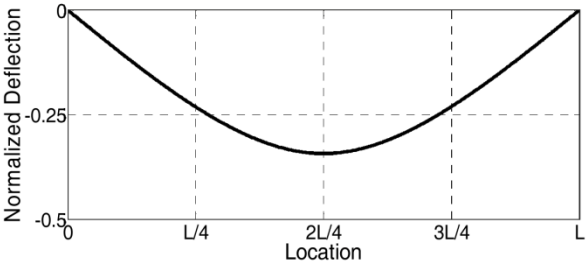

(g) Corrected deflection – 1st mode.

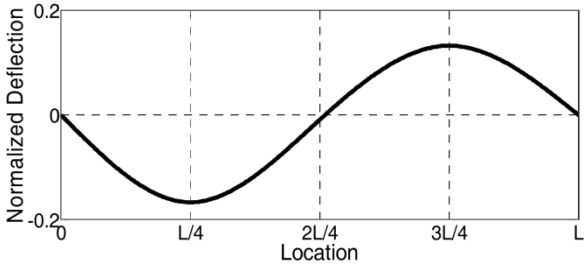

(h) Corrected deflection – 2nd mode.

Fig. 11 Mode shapes of curvature, slope and deflection along the ship length.

Fig. 12 compares the mode shapes of vertical bending moment, one obtained by the POD and the other one by the CRDT. For the first mode, the correspondence between the two results was almost perfect, but not for the second mode. The POD

slightly overestimated the bending moment at L/4 and underestimated it at 3L/4 compared to CRDT. As indicated before, the POM obtained by POD is an approximation of the eigenvector of the system so that one may conclude that the accuracy of CRDT is better than POD. The approximation nature of the POM to the mode shapes was attributed to the assumption of free vibration and uniform mass distribution. CRDT incorporates no artificial assumption; hence the accuracy is better than POD once the signal is filtered appropriately. On the other hand, filtering plays a key role in the accuracy of CRDT when the two vibration modes are closely related to the slight frequency gap, which may occur when the horizontal and torsional modes are present.

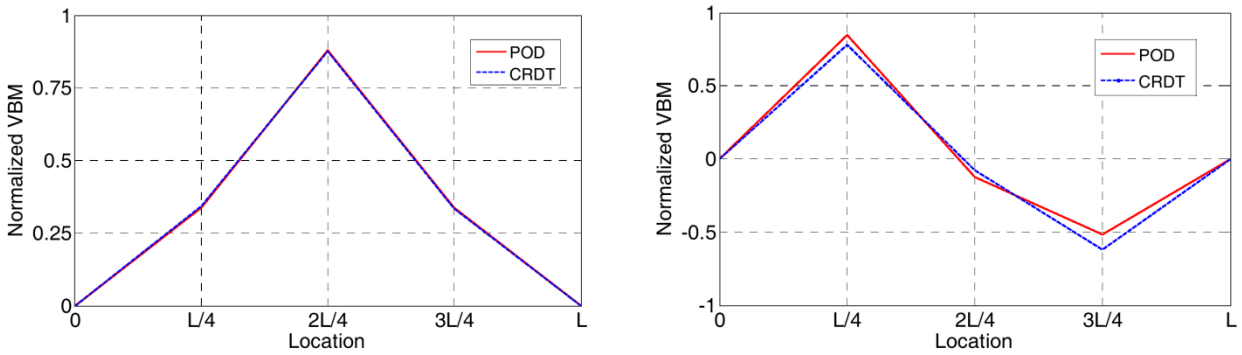

(a) 1st mode. (b) 2nd mode.

Fig. 12 VBM mode shape comparison between the POD and CRDT.

CONCLUSIONS

This paper addressed the prediction of mode shapes of a segmented hull model towed in a model basin using both the proper orthogonal decomposition and cross random decrement techniques. Based on the above discussions, the following conclusions were made.

- A segmented hull model of a 400 *K* ore carrier was towed in the model basin under an irregular wave load and the time series of the vertical bending moment was measured at L/4, 2L/4 and 3L/4 locations. The hydroelastic response was predominant in terms of the springing and whipping with its vibration frequencies of approximately 0.47 *Hz* and 1.07 *Hz*.
- The measure vertical bending moment time history was processed using the POD method and both the first and second vertical bending vibration modes were extracted. In addition, using the decomposed modal vectors, the measured vertical bending moment time history was decomposed into its first and second modes at three designated locations along the ship.
- The summation of the two decomposed vertical bending moment time histories matched the measured total vertical bending moment time history well. Moreover, error analysis of the POD method showed that the term, $\frac{1}{N} e_i^T e_j$, almost vanished when $i \neq j$, which confirmed the validity of the POM as an asymptotic approximation of the modal vector.
- The filtered vertical bending moment time history were processed using CRDT to obtain the free decay signal at three designated locations. The averaged signal converged quickly as the number of samples increased for both the first and second modes. The errors quickly decayed down and became less than 5% when the number of samples reached 100 for all cases but at 2L/4 in the second mode.
- The phase and magnitude difference of the free decay signal at the three designated locations revealed the mode shapes of the first and second vibrations. The mode shapes of the slope and deflection were also derived by numerically integrating the curvature and slope. The mode shapes of the deflection were in the form of well-known two and three-node vibrations.
- The mode shapes of the vertical bending moment obtained from both the POD and CRDT coincided well with each other. Some deviations between the two results were observed for the second mode shape, which can be attributed to the approximation nature of the POD, which assumes both a free vibration and uniform mass distribution.

ACKNOWLEDGEMENT

This study was supported by a Special Education Program for Offshore Plant by the Ministry of Trade, Industry and Energy Affairs (MOTIE). This research was also financially supported by Korea Evaluation institute of industrial technology (KEIT, Korea) and the Ministry of Trade, Industry & Energy (MOTIE, Korea) through the core technology development program of Industrial Convergence Technology (10045212, Predictive maintenance system for the integrated and intelligent operation of offshore plant). This work was supported by INHA UNIVERSITY Research Grant.

REFERENCES

Cole, H.A., 1968. On-the-line analysis of random vibrations. *AIAA Paper 68-288, 9th Structures, Structural Dynamics and Materials Conference*, Palm Springs, California.

Cole, H.A., 1971. *Method and apparatus for measuring the damping characteristics of a structure*. United States Patent No.3, 620,069.

DNV, 2000. *Environmental conditions and environmental loads, Classification Notes No.30.5*. Norway: DNV.

Drummen, I., Wu, M.K. and Moan, T., 2009.Experimental and numerical studyof containership responses in severe head seas. *Marine Structures*, 22(2), pp.172-193.

Feeny, B.F. and Kappagantu, R., 1998. On the physical interpretation of proper orthogonal modes in vibrations. *Journal of Sound and Vibration*, 211, pp.607-616.

Feeny, B.F., 2002. On proper orthogonal coordinates as indicators of modal activity. *Journal of Sound and Vibration*, 255, pp.805-817.

Hirdaris, S.E., Bakkers, N., White, N. and Temarel, P., 2009. Service factor assessment of a great lakes bulk carrier incorporating the effects of hydroelasticity. *Marine Technology*, 46(2), pp.116-121.

Hirdaris, S.E., Price, W.G. and Temarel, P., 2003. Two- and three-dimensional hydroelastic analysis of a bulker in waves. *Marine Structures Special issue on Bulk Carriers*, 16, pp.627-658.

Hong, S., Kim, B.W. and Nam, B.W., 2011. Experimental study on torsion springing and whipping of a large container ship. *In: Proceedings of the 21st International Offshore and Polar Engineering Conference*, Maui, Hawaii, USA, June 2011.

Ibrahim, S.R. and Mikulcik, E.C., 1977. A method for the direct identification of vibration parameter from the free response. *Shock and Vibration Bulletin*, 47(4), pp.183-198.

Iijima, K, Hermundstad, O.A., Zhu, S. and Moan, T., 2009. Symmetric and antisymmetric vibrations of a hydroelastically scaled model. *In: Proceedings of the 5th International Conference on Hydroelasticity in Marine Technology*, Southampton, UK, September 2009.

Jensen, J.J. and Dogliani, M., 1996. Wave-induced ship hull vibrations in stochastic seaways. *Marine Structures*, 9, pp.353-387.

Jensen, J.J., 2009. Stochastic procedures for extreme wave load predictions – wave bending moment in ships. *Marine Structures*, 22(2), pp.194-208.

Kim, K.H., Bang, J.S., Kim J.H., Kim, Y., Kim, S.J. and Kim, Y., 2013. Fully coupled BEM-FEM analysis for ship hydroelasticity in waves. *Marine Structures*, 33, pp.71-99.

Kim, Y. and Park, S.G., 2013. Wet damping estimation of the segmented hull model using the random decrement technique. *Journal of the Society of Naval Architects of Korea*, 50(4), pp.217-223.

Kim, Y., 2009. *Time domain analysis on hull-girder hydroelasticity by fully coupled BEM-FEM Approach*. PhD Thesis. Seoul National University.

Lumley, 1970. *Stochastic tools in turbulence*. New York: Academic Press.

Malenica, S., Molin, B. and Senjanovic, I., 2003. Hydroelastic response of a barge to impulsive and non-impulsive wave loads. *In: Proceedings of the 3rd International Conference on Hydroelasticity in Marine Technology*, Oxford, UK, September 2003.

Malenica, S., Senjanovic, I. and Vladimir, N., 2013. Hydro structural issues in the design of ultra large container ships. *Brodogradnja*, 64(3), pp.323-347.

Mariani, R. and Dessi, D., 2012. Analysis of the global bending modes of a floating structure using the proper orthogonal decomposition. *Journal of Fluids and Structures*, 28, pp.115-134.

Miyake, R., Matsumoto, T., Yamamoto, N. and Toyoda, K., 2010. On the estimation of hydroelastic response acting on an ultra-large container ship. *In: Proceedings of the 20th International Offshore and Polar Engineering Conference*, Beijing, China, September 2010.

Miyake, R., Matsumoto, T., Zhu, T., Usami, A. and Dobashi, H., 2009. Experimental studies on the hydroelastic response using a flexible mega-container ship model. *In: Proceedings of the 5th International Conference on Hydroelasticity in Marine Technology*, Southampton, UK, September 2009.

Oka, M., Oka, S. and Ogawa, Y., 2009. An experimental study on wave loads of a large container ship and its hydroelastic vibration. *In: Proceedings of the 5th International Conference on Hydroelasticity in Marine Technology*, Southampton, UK, September 2009.

Price, W.G. and Temarel, P., 1982. The influence of hull flexibility in the anti-symmetric dynamic behavior of ships in waves. *International Shipbuilding Progress*, 29.

Remy, F., Molin, B. and Ledoux, A., 2006. Experimental and numerical study of the wave response of a flexible barge. *In: Proceedings of the 4th International Conference on Hydroelasticity in Marine Technology*, Wuxi, China, September 2006.

Senjanovic, I., Vladimir, N., Tomic, M., Hadzic, N. and Malenica, S., 2014. Global hydroelastic analysis of ultra large container ships by improved beam structural model. *International Journal of Naval Architecture and Ocean Engineering*, 6(4), pp.1041-1063.

Wu, M.K. and Moan, T., 1996. Linear and nonlinear hydroelastic analysis of high-speed vessel. *Journal of Ship Research*, 40(2), pp.149-163.